EARLY OCEAN

Late inception of a resiliently oxygenated upper ocean

Wanyi Lu[1], Andy Ridgwell[2,3], Ellen Thomas[4,5], Dalton S. Hardisty[6], Genming Luo[7], Thomas J. Algeo[7,8,9], Matthew R. Saltzman[10], Benjamin C. Gill[11], Yanan Shen[12], Hong-Fei Ling[13], Cole T. Edwards[14], Michael T. Whalen[15], Xiaoli Zhou[1], Kristina M. Gutchess[1], Li Jin[16], Rosalind E. M. Rickaby[17], Hugh C. Jenkyns[17], Timothy W. Lyons[2], Timothy M. Lenton[18], Lee R. Kump[19], Zunli Lu[1]*

Rising oceanic and atmospheric oxygen levels through time have been crucial to enhanced habitability of surface Earth environments. Few redox proxies can track secular variations in dissolved oxygen concentrations around threshold levels for metazoan survival in the upper ocean. We present an extensive compilation of iodine-to-calcium ratios (I/Ca) in marine carbonates. Our record supports a major rise in the partial pressure of oxygen in the atmosphere at ~400 million years (Ma) ago and reveals a step change in the oxygenation of the upper ocean to relatively sustainable near-modern conditions at ~200 Ma ago. An Earth system model demonstrates that a shift in organic matter remineralization to greater depths, which may have been due to increasing size and biomineralization of eukaryotic plankton, likely drove the I/Ca signals at ~200 Ma ago.

The evolution and survival of marine animals depended on oxygen availability, particularly in upper ocean waters, ranging from the sea surface to the thermocline, during early Earth history (*1*). The dissolved oxygen concentration ($[O_2]$) in the upper ocean commonly decreases from the well-mixed surface ocean (the top few tens of meters) into deeper subsurface waters (a few hundred meters). This $[O_2]$ gradient is controlled by three key factors: (i) the partial pressure of oxygen in the atmosphere (P_{O_2}), (ii) the intensity of upper-ocean mixing, and (iii) the oxidation of organic matter in the water column, which consumes oxygen (*2*). Atmospheric P_{O_2} changes through time have been estimated via geochemical proxy data and box models (*3*). Oceanic paleoredox proxies typically track the areal extent of euxinic waters (containing H_2S) and the presence or absence of anoxia (positive or zero $[O_2]$) (*4*, *5*). Because most modern marine animals are sensitive to $[O_2]$ changes between ~10 and ~100 μmol/kg (*2*), development of long-term proxy reconstructions for $[O_2]$ in this critical range (oxic-hypoxic) would help elucidate when and how oceanic oxygenation evolved to accommodate the modern ecological landscape.

Carbonate I/Ca is one of the proxies developed for the oxic-hypoxic window that has the potential to reconstruct secular trends in upper-ocean oxygenation (*6*, *7*). The long residence time of iodine (~300,000 years) leads to generally uniform total iodine concentrations in the modern ocean, but speciation changes of iodine between iodate (IO_3^-) and iodide (I^-) are controlled locally (*8*, *9*). IO_3^- is completely reduced to I^- in waters at low $[O_2]$ (*8*, *9*) and reoxidized under well-oxygenated conditions. Because IO_3^- is the only chemical form of iodine incorporated into the carbonate structure (*7*) by replacing the CO_3^{2-} ion (*10*), carbonate I/Ca records of local seawater $[IO_3^-]$ through time can indicate changes in $[O_2]$. Carbonate I/Ca has been shown to be a reliable tracer that responds primarily to $[O_2]$ variations in marine environments over a wide range of geological periods (*6*, *11*–*16*).

We measured I/Ca in an extensive Phanerozoic collection of shallow marine carbonates likely forming within the top 200 m of the water column and compiled these values with published data (table S1 and Fig. 1A). Maximum I/Ca values for individual localities were generally low in the Proterozoic, except for periods that have been associated with potential atmospheric P_{O_2} rises [e.g., the Great Oxidation Event (*12*)] and some Neoproterozoic carbon isotope excursions (*11*, *15*), when maximum values temporarily increased to Cenozoic levels (3 to 4 μmol/mol) (Fig. 1A). Paleozoic maximum values are comparable to those of the Proterozoic, despite a relatively short spike during the Devonian, at about 400 million years (Ma) ago, when the 75th percentile values reached Cenozoic levels. Break-point analyses indicate a step change at Triassic to early Jurassic (~200 Ma ago, fig. S1), after which maximum values remain above 4 μmol/mol and 75th percentile values are mostly higher than 3 μmol/mol (*6*, *13*). The Devonian I/Ca excursion and the step change at ~200 Ma ago are two key observations in this data compilation.

The stark contrast between predominantly low Paleozoic values and high Meso-Cenozoic values (excluding the Triassic, i.e., <200 Ma ago) cannot be explained by sampling biases. The sample size for the Paleozoic (n = 894) is comparable to that for the Proterozoic (n = 1078) and the Meso-Cenozoic (n = 926). The sampling density (number of samples per unit time) is similar for the Paleozoic and Meso-Cenozoic, although lower in the Proterozoic (Fig. 1B). For Paleozoic samples, we targeted carbonate- and fossil-rich (shallow) continental-shelf locations, i.e., relatively well-oxygenated settings, which are prone to recording high I/Ca values. By contrast, many Mesozoic data were generated from sections recording well-established global oceanic anoxic events, which, if anything, would bias that dataset toward low values. Cenozoic I/Ca values were measured in sediment coarse fractions, which may better preserve primary I/Ca signatures than bulk-rock samples. Existing early Cenozoic (*14*) and Cretaceous I/Ca data (*13*) are generally comparable across different lithologies, although comparisons between the Cenozoic and other periods are more tenuous. The current dataset has relatively denser sample coverage for intervals coinciding with Earth system perturbations (e.g., major carbon-isotope excursions and mass extinctions) than for extended intervals with limited environmental changes, but this should not influence main features of the data compilation.

I/Ca values can potentially be reduced during subaerial exposure, marine burial, and dolomitization, but no postdepositional alterations are known to increase I/Ca (*11*). A variety of diagenesis indicators were considered in previous studies of samples that we used here (*7*, *15*–*17*). In all of those case studies, the number of potentially altered samples was limited and did not influence the central trend of most of the data through time, as represented by the 25th and 75th percentile values (Fig. 1A). High I/Ca values throughout the record (Fig. 1A) are not consistently tied to a specific inferred primary carbonate mineralogy (e.g., calcite versus aragonite seas, fig. S2A). The distinct behaviors of

[1]Department of Earth Sciences, Syracuse University, Syracuse, NY, USA. [2]Department of Earth Sciences, University of California, Riverside, Riverside, CA, USA. [3]School of Geographical Sciences, University of Bristol, Bristol, UK. [4]Department of Geology and Geophysics, Yale University, New Haven, CT, USA. [5]Department of Earth and Environmental Sciences, Wesleyan University, Middletown, CT, USA. [6]Department of Earth and Environmental Sciences, Michigan State University, East Lansing, MI, USA. [7]State Key Laboratory of Biogeology and Environmental Geology and School of Earth Science, China University of Geosciences, Wuhan, China. [8]State Key Laboratory of Geological Processes and Mineral Resources, China University of Geosciences, Wuhan, China. [9]Department of Geology, University of Cincinnati, Cincinnati, OH, USA. [10]School of Earth Sciences, The Ohio State University, Columbus, OH, USA. [11]Department of Geosciences, Virginia Polytechnic and State University, Blacksburg, VA, USA. [12]School of Earth and Space Sciences, University of Science and Technology of China, Hefei, China. [13]State Key Laboratory for Mineral Deposits Research, School of Earth Sciences and Engineering, Nanjing University, Nanjing, China. [14]Department of Geological and Environmental Sciences, Appalachian State University, Boone, NC, USA. [15]Department of Geosciences, University of Alaska, Fairbanks, Fairbanks, AK, USA. [16]Geology Department, State University of New York College at Cortland, Cortland, NY, USA. [17]Department of Earth Sciences, University of Oxford, Oxford, UK. [18]Earth System Science Group, College of Life and Environmental Sciences, University of Exeter, Exeter, UK. [19]Department of Geosciences, Pennsylvania State University, University Park, PA, USA.
*Corresponding author. Email: zunlilu@syr.edu

I/Ca before and after ~200 Ma ago (Fig. 1A) cannot be explained by secular changes in seawater [Ca^{2+}] (fig. S2B). No evidence suggests that differences in Paleozoic and Mesozoic I/Ca distributions were due to uniformly greater alteration of the Paleozoic samples (fig. S3). Lower relative standard deviations of neighboring samples in each section (i.e., smoother I/Ca profiles; fig. S4) may reflect better preservation of the Paleozoic than the Proterozoic samples (fig. S4).

We interpret I/Ca in marine carbonates primarily as a qualitative indicator for the depth of the oxycline (Fig. 2), that is, that part of the water column where the [O_2] decreases relatively abruptly. Carbonate rocks formed in the upper ocean record surface or near-surface seawater [IO_3^-], which is strongly affected by the presence or absence of a proximal oxygen minimum zone (OMZ) or a shallow oxycline. Owing to the relatively slow oxidation kinetics of I^- (*18*), surface waters may retain a low IO_3^- signal despite high in situ [O_2]. For instance, core-top (modern) planktonic foraminiferal shells exhibit low I/Ca values (~0.5 μmol/mol) in waters above a shallow OMZ in the equatorial Pacific but record higher values (>3 μmol/mol) at other well-oxygenated locations (*6*).

The large I/Ca excursion during the Devonian (Fig. 3) most likely reflects deepening of the oxycline and development of better oxygenated conditions in the upper ocean, consistent with published proxy data and modeling results (*4*, *5*, *19*, *20*). Although different box models yield somewhat divergent interpretations of atmospheric P_{O_2} variation through the Phanerozoic (*21*–*24*), a Devonian rise in P_{O_2} levels is plausible, on the basis of the carbon-oxygen-phosphorus-sulfur evolution (COPSE) model and charcoal proxy reconstructions (Fig. 3A), and was most likely due to increased abundance of vascular land plants (*19*, *20*). Previous work interpreted δ^{98}Mo, iron-speciation, and biological data (Fig. 3C) to reflect oceanic redox changes, supporting the idea of atmospheric P_{O_2} rise during the Devonian (*4*, *5*). The combination of these independent proxies indicates that the Devonian atmospheric P_{O_2} rise affected the whole atmosphere-ocean system, across the entire redox spectrum (Fig. 3).

I/Ca values returned to Proterozoic-like levels after the transient Devonian excursion, but there is no evidence for a P_{O_2} decrease to pre-Devonian levels between the Carboniferous and the Triassic. Instead, the post-Devonian atmosphere was probably relatively O_2 rich (Fig. 3A). High atmospheric P_{O_2} likely altered terrestrial weathering feedbacks and enhanced nutrient delivery to the ocean (*25*, *26*), leading to intensified O_2 consumption in the upper ocean, a generally shallow oxycline, and low I/Ca values between ~400 and 200 Ma ago (Fig. 3B). Under such conditions, carbonates formed in surface oceans rapidly equilibrated with the high-P_{O_2} atmosphere would record low in situ [IO_3^-] because of the slow oxidation of I^- during mixing between surface and subsurface waters (Fig. 2B). If the oxycline were indeed shallow, marine animals on continental shelves at that time (~400 to 200 Ma ago) would have been living in a thin layer of well-oxygenated surface water directly underlain by an OMZ (Fig. 2B). Our dataset (Fig. 1A) implies that well-oxygenated upper-ocean conditions became persistent and resilient only by the Triassic-Jurassic (~200 Ma ago), much later than previously inferred (*27*). The prerequisites for achieving such well-oxygenated upper-ocean conditions are a combination of high atmospheric P_{O_2} and a generally deep oxycline (Fig. 2C). The position of the oxycline is strongly controlled by the depth of organic-matter

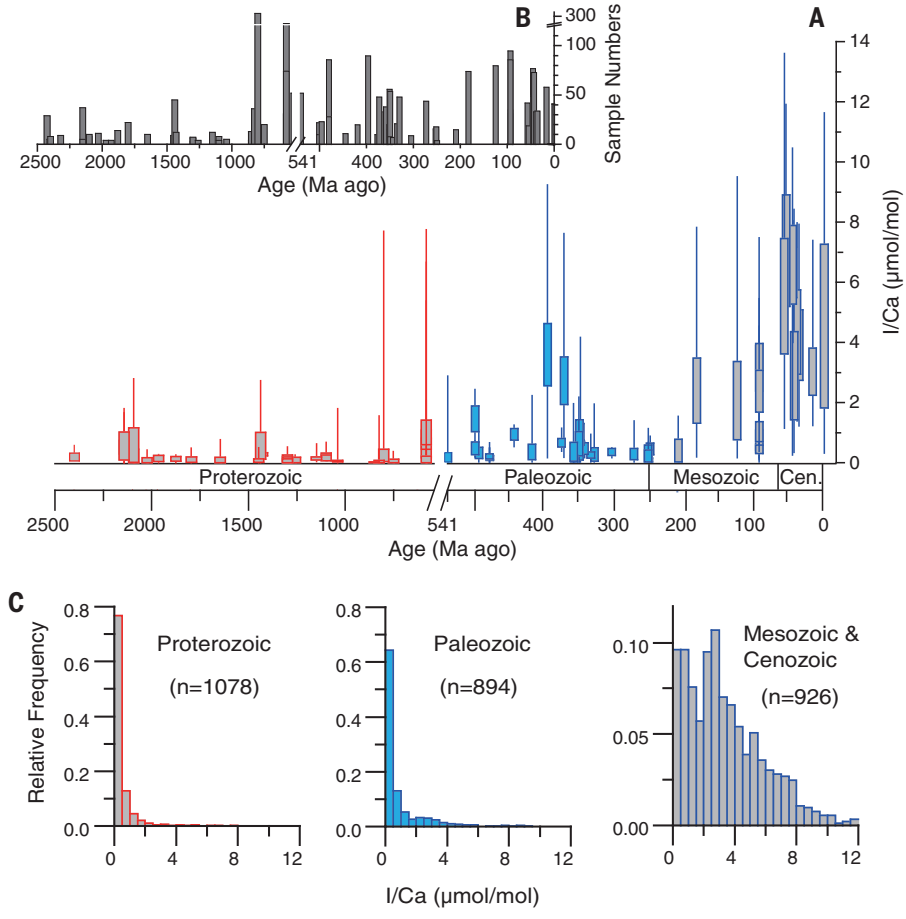

Fig. 1. Carbonate I/Ca through time. (**A**) Candlestick plot showing ranges of I/Ca values for Proterozoic (red) (*11*, *15*), Paleozoic (blue), and Meso-Cenozoic (purple). Boxes mark the 25th and 75th percentiles of values at each locality, and the whiskers show the maximum and minimum. The Proterozoic values from dolostones are I/(Mg + Ca). (**B**) Number of samples measured at each section. (**C**) Relative frequency distributions of I/Ca.

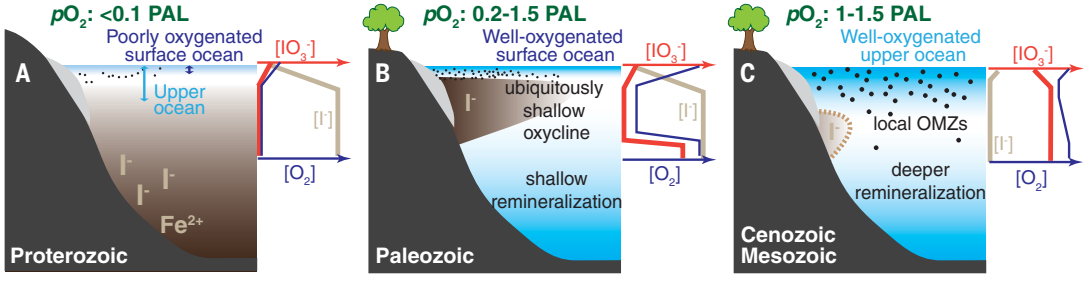

Fig. 2. Schematic illustrations for the evolution of oxygenation conditions. These simplified cartoons are not intended to capture all temporal and spatial variations. (**A**) Proterozoic. (**B**) Paleozoic. (**C**) Mesozoic and Cenozoic.

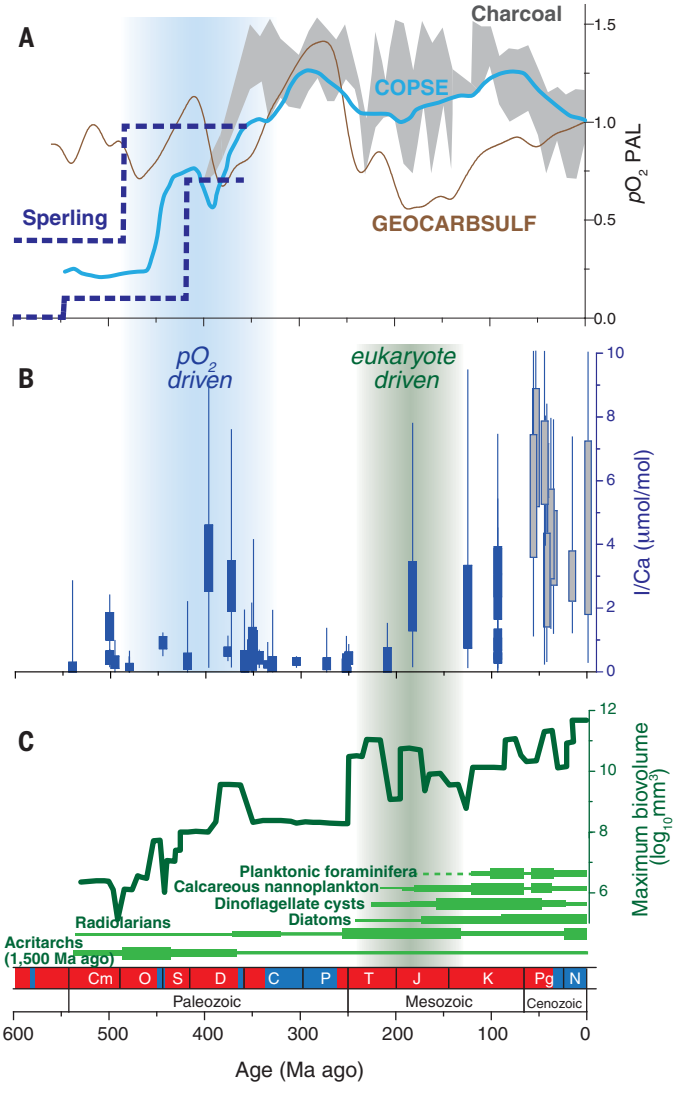

Fig. 3. Phanerozoic I/Ca compared with atmospheric P_{O_2}, oceanic oxygenation, and animal evolution trends. (**A**) Modeled atmospheric P_{O_2} curves (*5*, *21*, *23*, *24*) in comparison with the charcoal proxy record (*20*). Dashed lines (*5*) mark a broadly defined ocean-atmospheric O_2 level, not just atmospheric P_{O_2}. (**B**) I/Ca records through the Phanerozoic. Blue boxes indicate bulk carbonate rock; gray boxes indicate bulk coarse fraction of Ocean Drilling Project samples (>63 µm). (**C**) Marine animal body-size record (*36*). The thickness of the green bars indicates relative generic diversity modified from literature (*31*, *32*). The red versus blue bars mark greenhouse versus icehouse climate conditions, respectively. Cm, Cambrian; O, Ordovician; S, Silurian; D, Devonian; C, Carboniferous; P, Permian; T, Triassic; J, Jurassic; K, Cretaceous; Pg, Paleogene; N, Neogene.

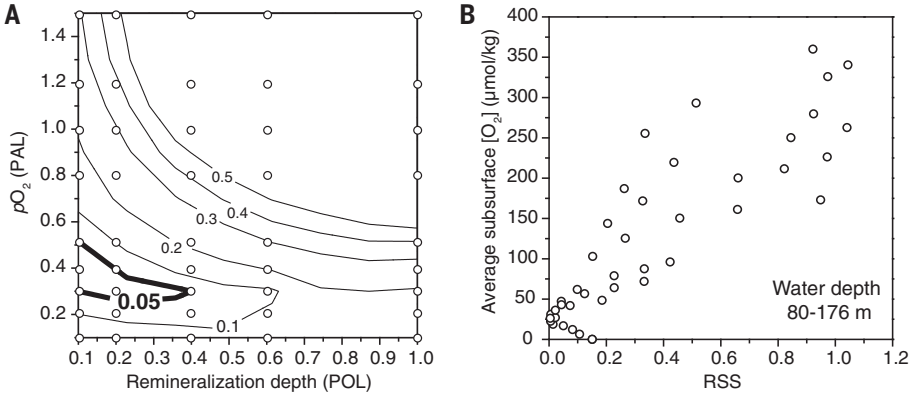

Fig. 4. Residual sum of squares and subsurface [O_2] at different P_{O_2} levels and remineralization depths. (**A**) Shallow remineralization depths produce the best model fit (the smallest RSS < 0.05) to Paleozoic I/Ca distribution, at 1x CO_2 condition. The circles represent 45 cGENIE simulations defining the contours. (**B**) Averaged [O_2] in the shallowest subsurface layer in each cGENIE run as an indicator of oxycline depth correlating with the RSS.

remineralization, which is dependent on the efficiency of organic-matter export from the photic zone, and has been proposed as a governing parameter for OMZs during the Phanerozoic (*28*).

We hypothesize that changes in remineralization of organic matter strongly influenced the upper-ocean I/Ca signature (Fig. 2), and we tested this hypothesis by simulating the marine iodine cycle in the cGENIE Earth system model (see methods and fig. S5) (*29*). We aimed to identify possible causes for low I/Ca during the Paleozoic through ensembles of model runs using a range of values for atmospheric P_{O_2}, the depth of organic-matter remineralization in the water column, and the mean concentrations of iodine and phosphate in seawater. For each Paleozoic model run, surface-water [IO_3^-] values along continental margins were extracted to calculate a relative frequency distribution (fig. S6). The modeled IO_3^- distributions were compared with observed Paleozoic I/Ca distributions (Fig. 1C) to obtain the residual sum of squares (RSS) (see materials and methods, Fig. 4A, and fig. S7).

We found that the lowest RSS values (<0.05), representing the best data-model fits, were achieved at shallow remineralization depths [i.e., <0.5 present oceanic level (POL)]. In the same set of cGENIE runs (Fig. 4B), lower RSS values correlated with lower average [O_2] in the subsurface layer (80 to 176 m), which is consistent with a shallower oxycline. Even as Paleozoic oceans experienced transitions between greenhouse and icehouse climate conditions, P_{CO_2} levels appear to have had minimal influence on IO_3^- distributions (fig. S8). Global-scale changes in ocean circulation and continent configuration also do not notably influence the oxycline depths independently of P_{O_2} and subsurface oxygen consumption (fig. S9). The RSS contours differed only slightly when the Paleozoic I/Ca distribution was compared with modeled [IO_3^-] distributions in the top four layers in the upper ocean (from 0 to 410 m, fig. S10). Thus, a lack of precise constraints on the paleodepths of carbonate formation is unlikely to have affected the main conclusions of our data-model comparison. Additional model runs also suggest that oceanic nutrient concentrations and total iodine concentrations are unlikely to dominate the secular trends in proxy data (figs. S11 and S12). Our data-model comparison (Fig. 4A) should not be viewed as a precise estimate of the atmospheric P_{O_2} for any single time slice, because the data were compiled over the entire Paleozoic under varying P_{O_2} levels. Thus, the lower RSS values at P_{O_2} below 1 present atmospheric level (PAL) suggest that some portions of the Paleozoic may have had P_{O_2} levels lower than those of today (*5*, *23*).

On the basis of our data compilation and model analyses, we attribute the transition at ~200 Ma ago from Proterozoic-like low I/Ca values in the Paleozoic (except for the mid-Devonian) to modern-like high values in the Meso-Cenozoic to a profound increase in the average remineralization depth of organic matter in the water column. The timing of this transition is consistent

with the proliferation of eukaryotic phyto- and zooplankton after the Permian-Triassic extinction (Fig. 3A) (*30*, *31*), which eventually shaped the ecological landscape of the modern ocean (*32*). The larger size of primary producers (*33*), grazing and repackaging of organic matter into fecal pellets (*34*), and/or the advent of mineralized plankton (*32*) may have led to faster sinking of organic matter, which reduced O_2 utilization in the upper water column and caused a pervasive deepening of the oxycline (*28*).

The rise of oxygen levels over geological time has been linked to increases in animal body size (*24*, *35*). A comprehensive compilation of Phanerozoic marine animal body-size data (*36*) shows that maximum biovolume probably covaried with I/Ca to some extent (Fig. 3B), indicating that O_2 availability in the global upper ocean may have been an important factor in Phanerozoic metazoan evolution. New forms of organisms (e.g., mineralized plankton, larger animals) fundamentally influenced oceanic environments, which in turn affected the evolving biosphere, representing a prime example of the coevolution of life and planet.

REFERENCES AND NOTES

1. A. H. Knoll, *Cold Spring Harbor Perspect. Biol.* **6**, a016121 (2014).
2. R. E. Keeling, A. Körtzinger, N. Gruber, *Ann. Rev. Mar. Sci.* **2**, 199–229 (2010).
3. T. W. Lyons, C. T. Reinhard, N. J. Planavsky, *Nature* **506**, 307–315 (2014).
4. T. W. Dahl *et al*., *Proc. Natl. Acad. Sci. U.S.A.* **107**, 17911–17915 (2010).
5. E. A. Sperling *et al*., *Nature* **523**, 451–454 (2015).
6. Z. Lu *et al*., *Nat. Commun.* **7**, 11146 (2016).
7. Z. Lu, H. C. Jenkyns, R. E. M. Rickaby, *Geology* **38**, 1107–1110 (2010).
8. G. W. Luther III, T. Campbell, *Deep-Sea Res. A, Oceanogr. Res. Pap.* **38**, S875–S882 (1991).
9. E. L. Rue, G. J. Smith, G. A. Cutter, K. W. Bruland, *Deep Sea Res. Part I Oceanogr. Res. Pap.* **44**, 113–134 (1997).
10. J. Podder *et al*., *Geochim. Cosmochim. Acta* **198**, 218–228 (2017).
11. D. S. Hardisty *et al*., *Earth Planet. Sci. Lett.* **463**, 159–170 (2017).
12. D. S. Hardisty *et al*., *Geology* **42**, 619–622 (2014).
13. X. Zhou *et al*., *Paleoceanography* **30**, 510–526 (2015).
14. X. L. Zhou, E. Thomas, R. E. M. Rickaby, A. M. E. Winguth, Z. L. Lu, *Paleoceanography* **29**, 964–975 (2014).
15. W. Lu *et al*., *Geochem. Perspect. Lett.* **5**, 53–57 (2017).
16. C. T. Edwards, D. A. Fike, M. R. Saltzman, W. Lu, Z. Lu, *Earth Planet. Sci. Lett.* **481**, 125–135 (2018).
17. G. R. Loope, L. R. Kump, M. A. Arthur, *Chem. Geol.* **351**, 195–208 (2013).
18. R. Chance, A. R. Baker, L. Carpenter, T. D. Jickells, *Environ. Sci. Process. Impacts* **16**, 1841–1859 (2014).
19. T. M. Lenton *et al*., *Proc. Natl. Acad. Sci. U.S.A.* **113**, 9704–9709 (2016).
20. I. J. Glasspool, A. C. Scott, *Nat. Geosci.* **3**, 627–630 (2010).
21. R. A. Berner, *Geochim. Cosmochim. Acta* **70**, 5653–5664 (2006).
22. N. M. Bergman, T. M. Lenton, A. J. Watson, *Am. J. Sci.* **304**, 397–437 (2004).
23. T. M. Lenton, S. J. Daines, B. J. Mills, *Earth Sci. Rev.* **178**, 1–28 (2018).
24. P. G. Falkowski *et al*., *Science* **309**, 2202–2204 (2005).
25. L. R. Kump, *Nature* **335**, 152–154 (1988).
26. T. J. Algeo, R. A. Berner, J. B. Maynard, S. E. Scheckler, *GSA Today* **5**, 64–66 (1995).
27. H. D. Holland, *Philos. Trans. R. Soc. London B Biol. Sci.* **361**, 903–915 (2006).
28. K. M. Meyer, A. Ridgwell, J. L. Payne, *Geobiology* **14**, 207–219 (2016).
29. A. Ridgwell *et al*., *Biogeosciences* **4**, 87–104 (2007).
30. M. E. Katz, Z. V. Finkel, D. Grzebyk, A. H. Knoll, P. G. Falkowski, *Annu. Rev. Ecol. Evol. Syst.* **35**, 523–556 (2004).
31. R. E. Martin, *Global Planet. Change* **11**, 1–23 (1995).
32. P. G. Falkowski *et al*., *Science* **305**, 354–360 (2004).
33. N. J. Butterfield, *Geobiology* **7**, 1–7 (2009).
34. G. A. Logan, J. M. Hayes, G. B. Hieshima, R. E. Summons, *Nature* **376**, 53–56 (1995).
35. J. L. Payne *et al*., *Photosynth. Res.* **107**, 37–57 (2011).
36. N. A. Heim, M. L. Knope, E. K. Schaal, S. C. Wang, J. L. Payne, *Science* **347**, 867–870 (2015).
37. W. Lu *et al*., (Table S2) I/Ca record of phanerozoic carbonates. PANGAEA (2018).

ACKNOWLEDGMENTS

Funding: We acknowledge funding from grants NSF EAR-1349252, OCE-1232620, and OCE-1736542 (Z.L.); NERC NE/J01043X/1, ERC-2013-CoG-617313, and NSF OCE-1736771 (A.R.); NSF OCE-1736538 (E.T.); National Key R&D Project of China 2016YFA0601104 and NSFC 41290260 (G.L.); NSFC 41330102 and 41721002 and the "111" project (Y.S.); Wolfson Research Merit award from the Royal Society and EU award (R.E.M.R.); and NERC NE/N018508/1 and NE/P013643/1 (T.M.L.). **Author contributions:** Z.L. conceived the study. W.L. and Z.L. carried out the data analysis, model simulations, and wrote the paper. A.R. modified cGENIE to incorporate the iodine cycle. All authors contributed to data interpretation and the writing of the manuscript. **Competing interests:** The authors declare that they have no competing interests. **Data and materials availability:** All I/Ca data are available in the supplementary materials. Table S2 is additionally provided online at www.pangaea.de/ (*37*).

SUPPLEMENTARY MATERIALS

www.sciencemag.org/content/361/6398/174/suppl/DC1
Materials and Methods
Figs. S1 to S12
References (*38*–*52*)
Tables S1 and S2

20 November 2017; accepted 17 May 2018
Published online 31 May 2018
10.1126/science.aar5372

Science

Late inception of a resiliently oxygenated upper ocean

Wanyi Lu, Andy Ridgwell, Ellen Thomas, Dalton S. Hardisty, Genming Luo, Thomas J. Algeo, Matthew R. Saltzman, Benjamin C. Gill, Yanan Shen, Hong-Fei Ling, Cole T. Edwards, Michael T. Whalen, Xiaoli Zhou, Kristina M. Gutchess, Li Jin, Rosalind E. M. Rickaby, Hugh C. Jenkyns, Timothy W. Lyons, Timothy M. Lenton, Lee R. Kump and Zunli Lu

Science **361** (6398), 174-177.
DOI: 10.1126/science.aar5372originally published online May 31, 2018

The rise of oxygen

To understand the evolution of the biosphere, we need to know how much oxygen was present in Earth's atmosphere during most of the past 2.5 billion years. However, there are few proxies sensitive enough to quantify O_2 at the low levels present until slightly less than 1 billion years ago. Lu *et al.* measured iodine/calcium ratios in marine carbonates, which are a proxy for dissolved oxygen concentrations in the upper ocean. They found that a major, but temporary, rise in atmospheric O_2 occurred at around 400 million years ago and that O_2 levels underwent a step change to near-modern values around 200 million years ago.

Science, this issue p. 174